

## A highly efficient Cu/AlOOH catalyst obtained by in situ reduction: Catalytic transfer hydrogenation of ML into $\gamma$ -GVL

Mingwei Ma<sup>a,1</sup>, Hui Liu<sup>a,1</sup>, Jingjie Cao<sup>a</sup>, Pan Hou<sup>a</sup>, Jiahui Huang<sup>b</sup>, Xingliang Xu<sup>c</sup>, Huijuan Yue<sup>a</sup>, Ge Tian<sup>a,\*</sup>, Shouhua Feng<sup>a</sup>

<sup>a</sup> State Key Laboratory of Inorganic Synthesis and Preparative Chemistry, College of Chemistry, Jilin University, Changchun 130012, PR China

<sup>b</sup> Dalian Institute of Chemical Physics, Chinese Academy of Sciences, Dalian 116023, PR China

<sup>c</sup> College of Chemistry and Material Science, Shandong Agricultural University, Taian 271018, PR China

### ARTICLE INFO

#### Keywords:

In situ reduced Cu/AlOOH  
Catalytic transfer hydrogenation  
Nanocatalyst  
Carbonyl compounds  
Zero-valent copper

### ABSTRACT

Catalytic transfer hydrogenation (CTH) of carbonyl compounds is considered as one of the most promising processes in the synthesis of fuels and chemicals. In this work, we propose a one-step strategy for catalyst preparation and CTH. Using the strategy, the production of  $\gamma$ -valerolactone ( $\gamma$ -GVL) was performed with isopropanol (2-PrOH) as solvent over in situ reduced nano-Cu/AlOOH catalyst from  $\text{Cu}_2(\text{OH})_2\text{CO}_3/\text{AlOOH}$  and the optimal reaction conditions for  $\gamma$ -GVL are 180 °C for 5 h using the in situ reduced catalyst with Cu/Al molar ratio 3/1 (90.51% yields of  $\gamma$ -GVL). Furthermore, it has been confirmed by different characterization methods (such as: SEM, TEM, XPS, etc.) that the catalyst is heterogeneous and exhibits high catalytic activity and stability which is attributed to the stability of the zero-valent copper in the catalyst and the nanosized particles of the catalyst. In addition, the catalysts also show general applicability to other carbonyl compounds.

### 1. Introduction

On account of limited natural sources and high demand, selective conversion of biomass to fuels and chemicals is important in the rapidly developing human society. [1,2] Among different methods for the conversion of biomass, catalytic routes are especially important and many biomass-derived chemicals and fuels can be produced by carefully designing catalytic systems [3].  $\gamma$ -Valerolactone ( $\gamma$ -GVL), one of the most promising platforms for the sustainable products of fuels and high value-added chemicals [4,5], can be synthesized by hydrogenolysis of levulinic acid (LA) or its esters from lignocellulosic biomass.

There are two different paths in the reactions. The first path is to use a series of metals (such as Pd, [6,7] Ru [8,9], Rh [10], Pt [11,12], Re [13], Ni [14–16], Co [17–19], Mo [20,21] and Cu [22,23]) as catalyst in the presence of molecular hydrogen ( $\text{H}_2$ ). [24,25] And the other one is accomplished under mild conditions [26] by using alcohols or formic acid (FA) and transition metal compounds instead of molecular hydrogen ( $\text{H}_2$ ) and precious metals as hydrogen sources and catalysts, respectively.

Recently, in the second path, the catalytic transfer hydrogenation (CTH) reaction, as a potential replacement to molecular hydrogen ( $\text{H}_2$ ),

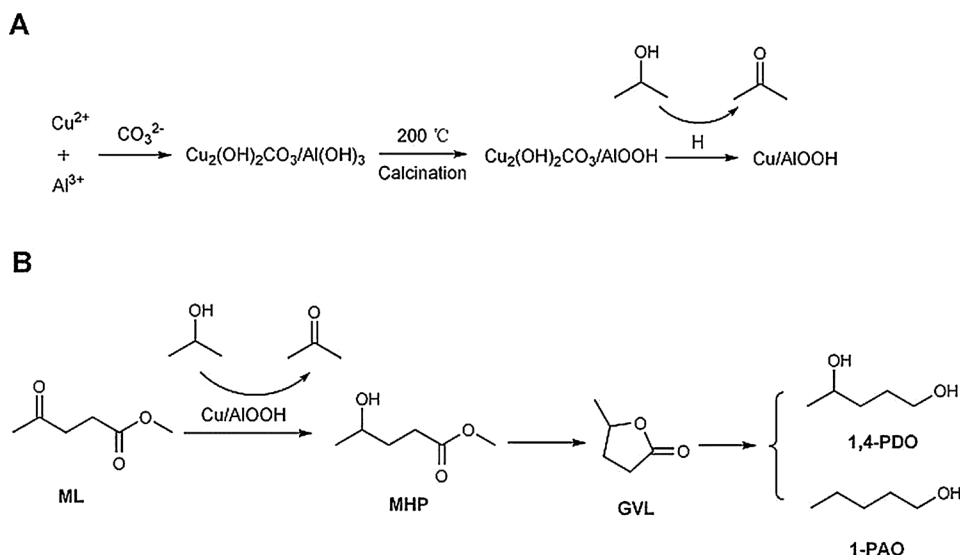
has been regarded as a high-efficiency route to synthesize  $\gamma$ -GVL from LA or its esters by using different alcohols as hydrogen source with various catalysts such as metal, [27,28] metal complexes [2,25,29], metal oxides or hydroxides [26,30,31], various zeolites [32], etc. In these catalysts, copper as a non-precious metal, combined with metal oxides, plays an important role in the synthesis of  $\gamma$ -GVL. Among these catalysts,  $\text{Cu}^0$  or metal oxides supported  $\text{Cu}^0$  as catalyst has been extensively studied and the relevant research results are summarized in Table S1. C. V. Rode et al. and Fu et al. researched copper-based catalysts for hydrogenation of LA into  $\gamma$ -GVL with  $\text{H}_2$  as a hydrogen source. [33,34] Huang et al. studied CTH reaction of EL into  $\gamma$ -GVL using alcohol as a hydrogen source over the Cu-Ni/ $\text{Al}_2\text{O}_3$  catalyst. [27] Lin et al. demonstrated for the first time that the catalytic hydrogenation of ML to  $\gamma$ -GVL in methanol with in situ reduced Cu or Cu/ $\text{Cr}_2\text{O}_3$  from CuO or CuO/ $\text{Cr}_2\text{O}_3$  as catalyst, which simplified the reaction by combining GVL production and catalyst synthesis into one step. [35,36] In the reaction, as a substitute for hydrogen, methanol reduces CuO to  $\text{Cu}^0$  above 200 °C, and it also catalyzes the synthesis of  $\gamma$ -GVL as a hydrogen source.

Some researches show that secondary alcohols have a stronger hydrogen supply capacity than primary alcohols at low temperatures. [4,37] And basic copper carbonate ( $\text{Cu}_2(\text{OH})_2\text{CO}_3$ ) is the compound

\* Corresponding author:

E-mail address: [tiange@jlu.edu.cn](mailto:tiange@jlu.edu.cn) (G. Tian).

<sup>1</sup> These authors contributed equally.



**Scheme 1.** Schematic for the in situ formation of the Cu/AlOOH catalyst with 2-PrOH as solvent (A). The possible reaction sequence for the conversion of ML into GVL, 1, 4-PDO and 1-PAO over the in situ reduced Cu/AlOOH catalyst (B).

most easily reduced by secondary alcohols among all copper sources below 200 °C (Scheme S1). Therefore, in this study, nano-Cu/AlOOH catalysts, prepared by in situ reduction of  $\text{Cu}_2(\text{OH})_2\text{CO}_3/\text{AlOOH}$  (Scheme 1A), efficiently participated in the CTH reaction from ML to  $\gamma$ -GVL with 2-PrOH as solvent (Scheme 1B). The high activity and stability of the catalyst are attributable to the stability of the zero-valent copper in the catalyst and the nanosized particles of the catalyst, which were proved by different characterization methods, such as: SEM, TEM, XPS, etc.

## 2. Experimental

### 2.1. Materials

Levulinic esters,  $\gamma$ -valerolactone, 1,4-pentanediol, 1-pentanol, furfural, furfuryl alcohol, 5-hydroxymethylfurfural, 2,5-bis(hydroxymethyl)furan, acetophenone,  $\alpha$ -phenylethyl alcohol, cyclohexanone, cyclohexanol, Citral, Citrate, cinnamaldehyde and cinnamyl alcohol were purchased from TCI Chemical Reagent Company (Shanghai, China).  $\text{Cu}(\text{NO}_3)_2 \cdot 6\text{H}_2\text{O}$ ,  $\text{Al}_2(\text{NO}_3)_3 \cdot 9\text{H}_2\text{O}$ ,  $\text{Na}_2\text{CO}_3$  and all solvents were purchased from Sinopharm Chemical Reagent Company (Shanghai, China). All chemicals were used without further purification.

### 2.2. Catalyst preparation

The  $\text{Cu}_2(\text{OH})_2\text{CO}_3/\text{AlOOH}$  catalyst with Cu/Al molar ratio of 3/1 were prepared by the co-precipitation method. Briefly,  $\text{Cu}(\text{NO}_3)_2 \cdot 6\text{H}_2\text{O}$  (15 mmol) and  $\text{Al}_2(\text{NO}_3)_3 \cdot 9\text{H}_2\text{O}$  (5 mmol) were dissolved in 40 mL deionized water and were stirred at ambient temperature for 15 min. With vigorous stirring, 1 M  $\text{Na}_2\text{CO}_3$  solvent was dropwise added until pH = 8. After being aged at room temperature for 5 h, the precipitate was separated by filtration and washed with deionized water several times. The precipitate obtained was dried overnight in the oven at 80 °C and then calcined at 200 °C for 5 h. Other Cu/Al molar ratios of  $\text{Cu}_2(\text{OH})_2\text{CO}_3/\text{AlOOH}$  catalyst (0, 1/5, 1/3, 1/1, 5/1,  $\infty$ ) were prepared in the same method.

$\text{CuO}/\text{Al}_2\text{O}_3$  for in situ reduction to produce  $\text{Cu}/\text{Al}_2\text{O}_3$  was prepared by baking the dried sample at 500 °C in an air atmosphere and hydrogen-reduced  $\text{Cu}/\text{Al}_2\text{O}_3$  catalyst was prepared by calcined  $\text{CuO}/\text{Al}_2\text{O}_3$  at 500 °C in a hydrogen atmosphere.

### 2.3. CTH reaction and sample analysis

CTH reaction of ML was performed without stirring in a steel alloy autoclave (Fe-Cr-Ni alloy, GB1220-92) with an internal volume of 35 ML. Typically, carbonyl compounds (0.67 mmol), solvents (20 mL), and catalyst (0.1 g) were charged into the reactor, which was then sealed and heated to a designed temperature (140–220 °C) for an intended reaction time (1–24 h). After the reaction, the autoclave was taken out and cooled to ambient temperature.

Identification of liquid products in the reaction mixture was achieved by the TRACE ISQ GC-MS (Thermo Scientific Co, TR-WAX-MS column 30.0 m  $\times$  320  $\mu\text{m}$   $\times$  0.25  $\mu\text{m}$ ). The temperature program started at 60 °C for 1 min, then increased from 60 °C to 230 °C at a rate of 15 °C /min and held for 2 min.

### 2.4. Catalyst characterization

X-ray diffraction (XRD) was carried out via a Rigaku D/max-2550 diffractometer using Cu-K $\alpha$  radiation. The wavelength of X-ray source was set at 0.154 nm, and the step width was 0.02° with a scanning speed of 6° per minute between two theta of 10° and 80°. Fourier transform infrared (FT-IR) spectra were recorded between 400 to 4000  $\text{cm}^{-1}$  by using Bruker VERTEXV 80 V spectrometer. The thermogravimetric (TG) analysis was performed using a thermogravimetric analysis system (TG: PerkinElmer Instruments) under air atmosphere at the heating rate of 10 °C  $\text{min}^{-1}$ . Brunauer -Emmett-Teller (BET) surface area was measured on an Asap 2420 surface adsorption apparatus. The elemental compositions of catalysts were determined by inductively coupled plasma (ICP) on an Optima 3300 DV (PerkinElmer Instruments).  $\text{NH}_3$ -TPD and  $\text{CO}_2$ -TPD (temperature-programmed desorption) were conducted on a Micromeritics AutoChem I2920 automated chemisorption analyzer to assess the surface acidity and basicity of catalysts, respectively. X-ray photoelectron spectroscopy (XPS) measurements were performed using ESCALAB250 photoelectron spectrometer equipped with a charge neutralizer and an Mg K $\alpha$  X-ray source. The morphology of the samples was investigated by transmission electron microscopy (TEM; Tecnai F20) and scanning electron microscopy (SEM; Jeol JSM-6700 F).

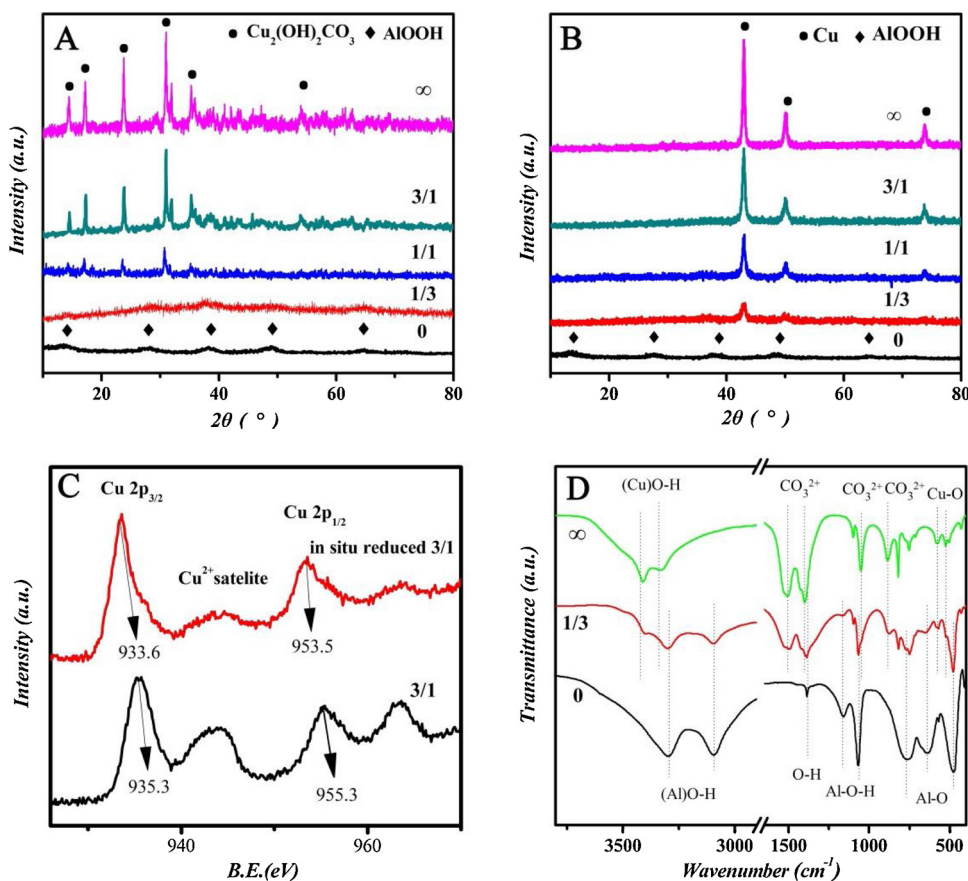


Fig. 1. The characterization of catalysts with different Cu/Al molar ratios. XRD patterns of  $\text{Cu}_2(\text{OH})_2\text{CO}_3/\text{AlOOH}$  with different Cu/Al molar ratios (A). XRD patterns of in situ reduced catalysts with different Cu/Al molar ratios after the reaction (B). XPS spectra of  $\text{Cu}_2(\text{OH})_2\text{CO}_3/\text{AlOOH}$  and in situ reduced catalysts with 3/1 ratio of Cu/Al (C). FT-IR spectra of  $\text{Cu}_2(\text{OH})_2\text{CO}_3/\text{AlOOH}$  with different Cu/Al molar ratios (D).

### 3. Results and discussion

#### 3.1. Characterization of catalysts

$\text{Cu}_2(\text{OH})_2\text{CO}_3/\text{AlOOH}$  catalysts were designed with Cu/Al molar ratios of 0, 1:3, 1:1, 3:1 and  $\infty$  (100% copper). And ICP results demonstrate that the real Cu/Al molar ratios is consistent with the theoretical value (Table S2). In a series of  $\text{Cu}_2(\text{OH})_2\text{CO}_3/\text{AlOOH}$  catalysts with different Cu/Al molar ratios, the surface areas, pore volume and pore size of the catalysts were determined by BET, and the results reveal that the catalysts have a rich pore structure. Furthermore, surface area of the catalysts decreases as the Cu/Al molar ratio increases. (Table S3 and Figure S1 A).

XRD patterns of  $\text{Cu}_2(\text{OH})_2\text{CO}_3/\text{AlOOH}$  with different Cu/Al molar ratios are presented in Fig. 1A. When the Cu/Al molar ratio is 0 and 1/3, XRD patterns only indicate the faint characteristic peak of AlOOH ( $2\theta = 14.5^\circ, 28.2^\circ, 38.3^\circ, 48.9^\circ$  and  $64.9^\circ$ , PDF, 21–1307). With the increase of Cu/Al ratio from 1/1 to  $\infty$ , the characteristic peaks of  $\text{Cu}_2(\text{OH})_2\text{CO}_3$  ( $2\theta = 14.8^\circ, 17.5^\circ, 24.0^\circ, 31.2^\circ, 35.6^\circ$  and  $54.8^\circ$ , PDF, 41–1390) strengthens, while the peak of AlOOH becomes weak or disappears due to its low crystallinity or low content, which is also the reason that no  $\text{Cu}_2(\text{OH})_2\text{CO}_3$  peak exists in the pattern of the catalyst with 1/3 ratio of Cu/Al. In Fig. 1B, XRD patterns of in situ reduced catalysts with different molar ratios after the reaction are recorded and metallic Cu is acquired. Except the catalyst with 0 ratio of Cu/Al, all catalysts show the characteristic peaks of metallic Cu ( $2\theta = 43.2^\circ, 50.4^\circ$  and  $74.1^\circ$ , PDF, 04-0836). At the same time, it can be observed that as the Cu/Al proportion increases, the intensity of Cu peak increases. And no obvious diffraction peaks of AlOOH was observed in the XRD patterns except for the catalyst with 0 ratio of Cu/Al, attributed to its low crystallinity or low content. Therefore, we can draw preliminary conclusions that Cu/AlOOH is generated by in situ reduction of  $\text{Cu}_2(\text{OH})_2\text{CO}_3/\text{AlOOH}$  after catalytic transfer hydrogenation (CTH) of

ML into  $\gamma$ -GVL. Apart from this, the XPS analysis further proved this view (Fig. 1C). For Cu  $2p_{3/2}$  and Cu  $2p_{1/2}$ , in situ reduced samples have lower binding energy than  $\text{Cu}_2(\text{OH})_2\text{CO}_3/\text{AlOOH}$ , demonstrating that  $\text{Cu}^{2+}$  species were reduced to Cu or  $\text{Cu}^+$  species after the CTH reaction. Meanwhile,  $\text{Cu}^{2+}$  satellite peak becomes weaker, apparently confirmed that more  $\text{Cu}^{2+}$  species were reduced to Cu or  $\text{Cu}^+$  species. In addition, the XPS peaks of Cu  $2p_{3/2}$  were deconvoluted to explore Cu species in different valence states (Figure S2), and  $\text{Cu}^{2+}$  is obviously reduced to Cu or  $\text{Cu}^+$  after the reaction. The fact that Cu/AlOOH can be prepared by in situ reduced method in the process of CTH reaction is proved.

The FT-IR analysis (Fig. 1D) clearly reveals the characteristic absorption peaks of  $\text{Cu}_2(\text{OH})_2\text{CO}_3$  and AlOOH. For the  $\text{Cu}_2(\text{OH})_2\text{CO}_3$  [38,39], the peaks at  $3416$  and  $3343\text{ cm}^{-1}$  are assigned to the (Cu) O–H stretching modes. The two vibration peaks appearing at  $1508$  and  $1401\text{ cm}^{-1}$  arise from the asymmetric stretching vibration of  $\text{CO}_3^{2-}$ . The peaks at  $1055$  and  $880\text{ cm}^{-1}$  can be attributed to the symmetric stretching and out of plane bending vibrations of  $\text{CO}_3^{2-}$ , respectively. The peaks at  $588$  and  $531\text{ cm}^{-1}$  are assigned to the Cu–O stretching modes. For the AlOOH, [40–42] the two peaks at  $3297$  and  $3091\text{ cm}^{-1}$  are assigned to the symmetrical and asymmetrical stretching vibrations of (Al)O–H groups respectively. The peak at  $1381\text{ cm}^{-1}$  is attributed to the OH bending vibration. The absorption peaks at  $1068$  and  $1162\text{ cm}^{-1}$  correspond to the symmetric and asymmetric bending vibrations of Al–OH, respectively. And the three characteristic peaks at  $762$ ,  $641$ , and  $480\text{ cm}^{-1}$  were ascribed to the vibration mode of Al–O. The above results verify that the composition of catalyst is  $\text{Cu}_2(\text{OH})_2\text{CO}_3$  and AlOOH.

From TG/DTA analysis (Figure S1B), the temperature range of  $\text{NH}_3$ -TPD and  $\text{CO}_2$ -TPD tests are determined to be between  $100^\circ\text{C}$  and  $310^\circ\text{C}$  (Figure S1 C–F). Figure S1C presents the  $\text{NH}_3$ -TPD profiles with various Cu/Al molar ratio samples, which indicates that all samples exhibit a medium strong acidic site at around  $300^\circ\text{C}$ , especially high Cu/Al molar ratio catalysts (3/1 and  $\infty$ ). After the in situ reduction, the

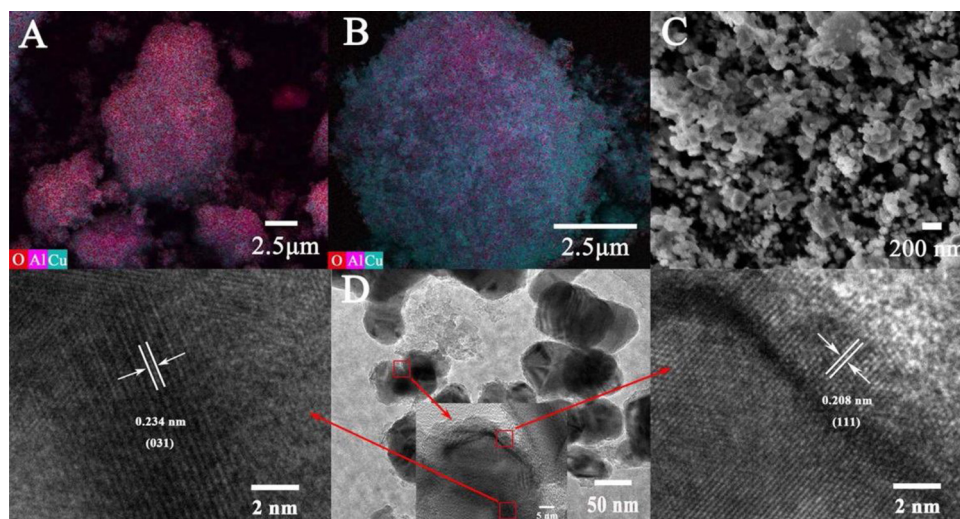


**Fig. 2.** The characterization of the  $\text{Cu}_2(\text{OH})_2\text{CO}_3/\text{AlOOH}$  and the  $\text{Cu}/\text{AlOOH}$ . SEM-EDS elemental mapping images of the  $\text{Cu}_2(\text{OH})_2\text{CO}_3/\text{AlOOH}$  with a Cu/Al molar ratio of 3/1 (A). SEM-EDS elemental mapping images (B), SEM images (C) and TEM image (D) of the  $\text{Cu}/\text{AlOOH}$  with a Cu/Al molar ratio of 3/1.

catalyst maintains medium strong acid sites (300 °C). The results from  $\text{CO}_2$ -TPD analysis is similar to the results of  $\text{NH}_3$ -TPD analysis, there are large amounts of basic sites in the  $\text{Cu}/\text{AlOOH}$ , which meet the need for acidic and basic sites of the catalysts in the CTH reaction of LA or its esters.

Microstructure of samples was further monitored by SEM, TEM and HRTEM. From the Fig. 2A and B, we can conclude that the distribution of O, Al and Cu elements in the sample is very uniform before and after the in situ reduction. In particular, the  $\text{Cu}/\text{AlOOH}$  after in situ reduction have more blue bright spots than before the reaction, which is due to the reduction of O element resulted by the decomposition of  $\text{Cu}_2(\text{OH})_2\text{CO}_3$  and the in situ reduced Cu accumulated on the surface of the particles. In addition, the catalyst shows a good dispersion of O, Al and Cu elements (Figure S3), and an average particle size of nano-Cu/ $\text{AlOOH}$  after in situ reduction is about 30–40 nm (Fig. 2C and D). Further analysis, The HRTEM image highlights a typical metallic Cu with a lattice space of 0.208 nm, which is assigned to the (111) plane of metallic Cu and a typical  $\text{AlOOH}$  with a lattice space of 0.234 nm, which is assigned to the (031) plane of  $\text{AlOOH}$ . Similarly, the fact that  $\text{Cu}/\text{AlOOH}$  can be prepared by in situ reduced method in the process of CTH reaction is also confirmed.

### 3.2. Catalytic activity of the various copper - aluminum catalysts for the CTH of ML

In our research, ML was used as a model reactant to study the activity of various copper - aluminum catalysts for the production of  $\gamma$ -GVL through the CTH reaction. No reaction happened in the absence of any catalyst (Table 1, entry 1). With the Cu/Al molar ratio of the catalyst increasing from 0 to  $\infty$ , the conversion of ML and the yield of the products all become volcano-like (Table 1, entry 2–8), and the best catalytic performance is exhibited with Cu/Al molar ratio 3/1. The yields of  $\gamma$ -GVL and 1,4-PDO at this time were 90.51% and 3.47% at 180 °C with 5 h, respectively. This phenomenon can be seen more clearly from the 3D figure (Figure S4). Both the physically mixed  $\text{Cu}_2(\text{OH})_2\text{CO}_3/\text{AlOOH}$  catalyst and the uncalcined catalyst showed lower catalytic activity, and the yields of  $\gamma$ -GVL were 47.95% and 81%, respectively (Table 1, entry 9–10). The former was caused by inhomogeneous mixing of  $\text{Cu}_2(\text{OH})_2\text{CO}_3$  and  $\text{AlOOH}$ , and the latter was affected by the support of  $\text{Al}(\text{OH})_3$  in the catalyst, possibly due to the lower amount of catalytically active sites than  $\text{AlOOH}$  in the same mass of catalyst. Finally, we compared the in situ reduced of  $\text{Cu}/\text{AlOOH}$  and the in situ reduced  $\text{Cu}/\text{Al}_2\text{O}_3$  in the CTH of ML (Table 1, entry 11). On

**Table 1**

CTH reaction of ML with isopropanol over various Cu/Al molar ratio catalysts and related catalysts.

Entry	Cu/Al molar ratio	$N_{\text{Cu}}$ (mmol)	Catalyst	Conv (%)	GVL Yield (%)	1,4-PDO Yield (%)
1 <sup>[a]</sup>	0	0	0	3.02	0.17	0
2	0	0	$\text{AlOOH}$	33.02	26.56	0
3	1/5	0.24	$\text{Cu}_2(\text{OH})_2\text{CO}_3/\text{AlOOH}$	89.33	81.89	1.85
4	1/3	0.34	$\text{Cu}_2(\text{OH})_2\text{CO}_3/\text{AlOOH}$	90.26	84.48	2.71
5	1/1	0.58	$\text{Cu}_2(\text{OH})_2\text{CO}_3/\text{AlOOH}$	93.14	86.48	3.22
6	3/1	0.76	$\text{Cu}_2(\text{OH})_2\text{CO}_3/\text{AlOOH}$	96.07	90.51	3.47
7	5/1	0.81	$\text{Cu}_2(\text{OH})_2\text{CO}_3/\text{AlOOH}$	91.65	84.64	2.16
8	$\infty$	—	$\text{Cu}_2(\text{OH})_2\text{CO}_3$	30.56	11.02	0
9 <sup>[b]</sup>	3/1	0.76	$\text{Cu}_2(\text{OH})_2\text{CO}_3/\text{AlOOH}$	75.26	47.95	0.77
10 <sup>[c]</sup>	3/1	—	Uncalcined	85.39	81.89	2.33
11 <sup>[d]</sup>	3/1	1 (0.76)	$\text{CuO}/\text{Al}_2\text{O}_3$	> 99 (89.86)	77.45 (82.22)	14.56 (2.42)
12 <sup>[e]</sup>	3/1	1.23	$\text{Cu}/\text{Al}_2\text{O}_3(\text{H}_2)$	88.17	77.95	3.86

Conditions: catalyst(0.1 g), substrate(0.67 mmol), 2-PrOH (20 mL), 180 °C, 5 h. [a] Reaction without any catalyst. [b] Physical mixture of  $\text{Cu}_2(\text{OH})_2\text{CO}_3$  and  $\text{AlOOH}$  with a Cu/Al molar ratio of 3/1. [c]  $\text{Cu}_2(\text{OH})_2\text{CO}_3/\text{Al}(\text{OH})_3$  is not calcined at 200 °C. [d] The data in parentheses is 0.063 g  $\text{CuO}/\text{Al}_2\text{O}_3$  that is calcined at 500 °C for 5 h (0.76 mmol  $\text{Cu}^{2+}$ ). [e]  $\text{CuO}/\text{Al}_2\text{O}_3$  is reduced under  $\text{H}_2$  atmosphere at 500 °C for 5 h.

account of the large amount of copper (1 mmol), the in situ reduced  $\text{Cu}/\text{Al}_2\text{O}_3$  catalyst displayed a very good catalytic effect (> 99% conversion of ML and 77.45% yield of GVL). Further, the amount of the catalyst was reduced to containing 0.76 mmol of copper, which is the same as the number of moles of copper in the  $\text{Cu}_2(\text{OH})_2\text{CO}_3/\text{AlOOH}$  catalyst with Cu/Al molar ratio 3/1, and their catalytic activities under the same conditions were compared. The results showed that the catalytic activity of in situ reduced  $\text{Cu}/\text{Al}_2\text{O}_3$  catalyst is lower than that of  $\text{Cu}/\text{AlOOH}$  catalyst with the same molar number of copper (Table 1, entry 6 and 11). This is because  $\text{Cu}_2(\text{OH})_2\text{CO}_3$  is easier to be reduced to zero

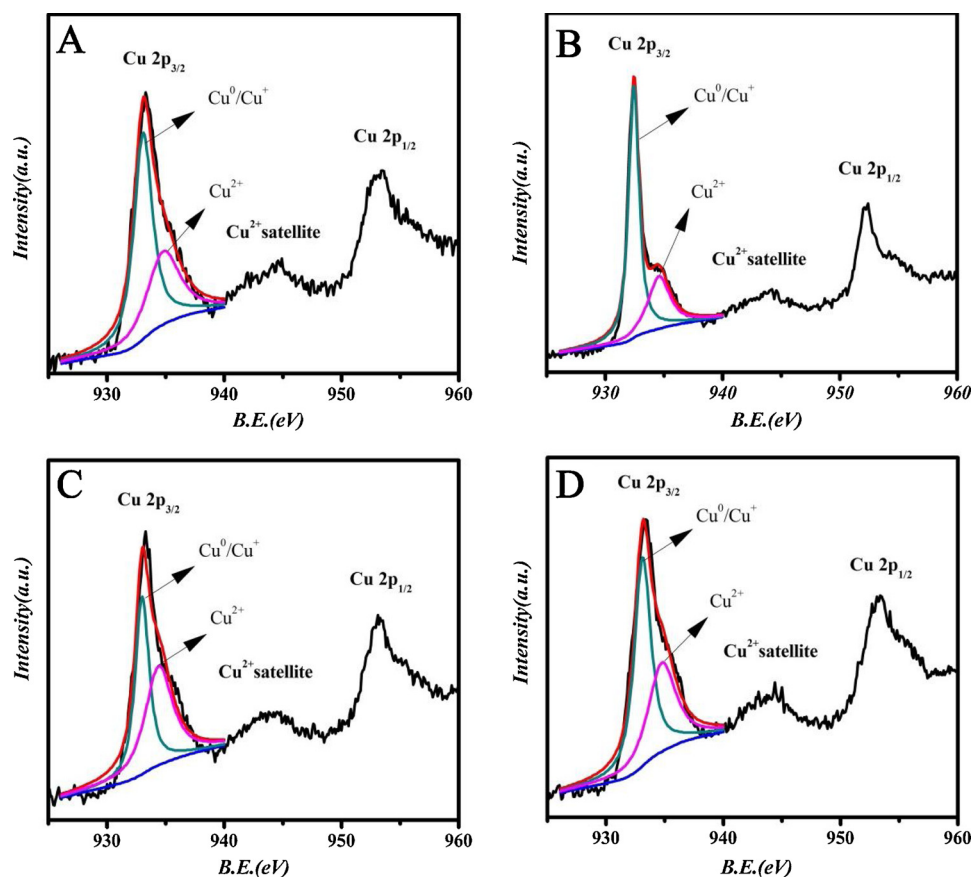


Fig. 3. XPS analysis of the in situ reduced Cu/AlOOH (A), in situ reduced Cu/Al<sub>2</sub>O<sub>3</sub> (B), hydrogen-reduced Cu/Al<sub>2</sub>O<sub>3</sub> (C) and spent hydrogen-reduced Cu/Al<sub>2</sub>O<sub>3</sub> (D).

valence copper than CuO in a shorter time (1 h and 3 h), which is proved by XRD (Figure S5 A and Figure S5C). By comparing the in situ reduced catalyst with the hydrogen-reduced catalyst (Table 1, entry 12), it is found that the hydrogen-reduced Cu/Al<sub>2</sub>O<sub>3</sub> has lower catalytic activity, which is attributed to the agglutination of the particles of the catalyst (Figure S6).

From ICP results (Table S2) and XRD patterns (Figure S5B) of the hydrogen-reduced Cu/Al<sub>2</sub>O<sub>3</sub> and CuO/Al<sub>2</sub>O<sub>3</sub> before and after in situ reduction, the actual Cu/Al molar ratio is in line with the theoretical value and CuO/Al<sub>2</sub>O<sub>3</sub> can be reduced by in situ reduction as expected. From the SEM images of in situ reduced Cu/Al<sub>2</sub>O<sub>3</sub> (Figure S6 A) and hydrogen-reduced Cu/Al<sub>2</sub>O<sub>3</sub> (Figure S6B), we can clearly observe that the in situ reduced catalyst has good dispersibility while the hydrogen-reduced catalyst particles tend to aggregate, which may be the reason for its low catalytic activity. To explore further the influence of the chemical state of the metal on the reaction, XPS analysis of the various catalysts was accomplished (Fig. 3). The main peak of Cu 2p<sub>3/2</sub> at 932.4 eV corresponded to the Cu<sup>0</sup>/Cu<sup>+</sup> species because the binding energies of Cu<sup>0</sup> and Cu<sup>+</sup> in Cu 2p<sub>3/2</sub> were extremely close. The peak at 934.2 eV, together with its satellite peak around 944 eV, was attributed to the Cu<sup>2+</sup> species. [43,44] Comparing Fig. 3A, B, and C, the deconvolution of the Cu 2p<sub>3/2</sub> peak was determined to be about 1.62:1, 2.35:1 and 0.91:1 for Cu<sup>0</sup>/Cu<sup>+</sup>: Cu<sup>2+</sup>, respectively, indicating that the in situ reduced Cu/AlOOH and Cu/Al<sub>2</sub>O<sub>3</sub> has more Cu<sup>0</sup>/Cu<sup>+</sup> species than the hydrogen-reduced Cu/Al<sub>2</sub>O<sub>3</sub> and therefore have a better catalytic performance. As a result of reducibility of 2-PrOH, the quantity of Cu<sup>0</sup>/Cu<sup>+</sup> species increased in spent hydrogen-reduced Cu/Al<sub>2</sub>O<sub>3</sub> after the reaction (Fig. 3D). From the XPS analysis, the conclusion was drawn that high catalytic activity of the in situ reduced catalysts was caused by high concentration of low chemical state in Cu species, the result was achieved by the in situ reduction of 2-PrOH as a hydrogen source.

### 3.3. Effect of reaction temperature and time

The influence of reaction temperature and time on the production of  $\gamma$ -GVL, 1,4-PDO and 1-PAO from ML was studied, and all experiments were conducted at 140 °C, 160 °C, 180 °C, 200 °C and 220 °C with the reaction time in the range of 1 to 24 h, respectively. It can be seen that the effect of temperature and time on the reaction is remarkable. From Fig. 4A–E, we can see that as the temperature increases, the reaction time to achieve the highest yield of  $\gamma$ -GVL is significantly reduced (from 24 h at 140 °C to 1 h at 220 °C). Comprehensive temperature and time factors, the optimal reaction condition of  $\gamma$ -GVL is 180 °C and 5 h. In addition, the optimal reaction condition of 1, 4-PDO, the further product of  $\gamma$ -GVL, is 200 °C for 5 h with 28.36% yield. The reaction temperature and time are continuously increased (220 °C and 24 h), the reaction will further generate 1-PAO with the best yield of 9.27%, which possibly due to the hydrogenolysis of 1, 4-PDO.

Through further XRD and XPS analysis, we can infer the effect of time on in situ reduction, and then the impact on the reaction. From Figure S5C, the Cu<sub>2</sub>(OH)<sub>2</sub>CO<sub>3</sub> in the samples was partially reduced to metallic Cu at 1 h. As time increases, the samples were completely reduced to Cu after 3 h. Further integration Figure S5D, the phenomenon that the peak positions of Cu 2p<sub>3/2</sub> and Cu 2p<sub>1/2</sub> shift toward low binding energy with the increase of time indicates that more and more Cu<sup>2+</sup> is reduced to Cu<sup>+</sup> or Cu<sup>0</sup> over time and the trend of smaller satellite peaks of Cu 2p<sub>3/2</sub> also confirms this view. Therefore, it can be demonstrated that the time influences the degree of in situ catalyst synthesis, which in turn affects the CTH reaction of ML.

### 3.4. Effect of the catalyst dosage

Effect of the catalyst dosage on the CTH reaction of ML was researched (Fig. 4F). It was evident that both the conversion of ML and

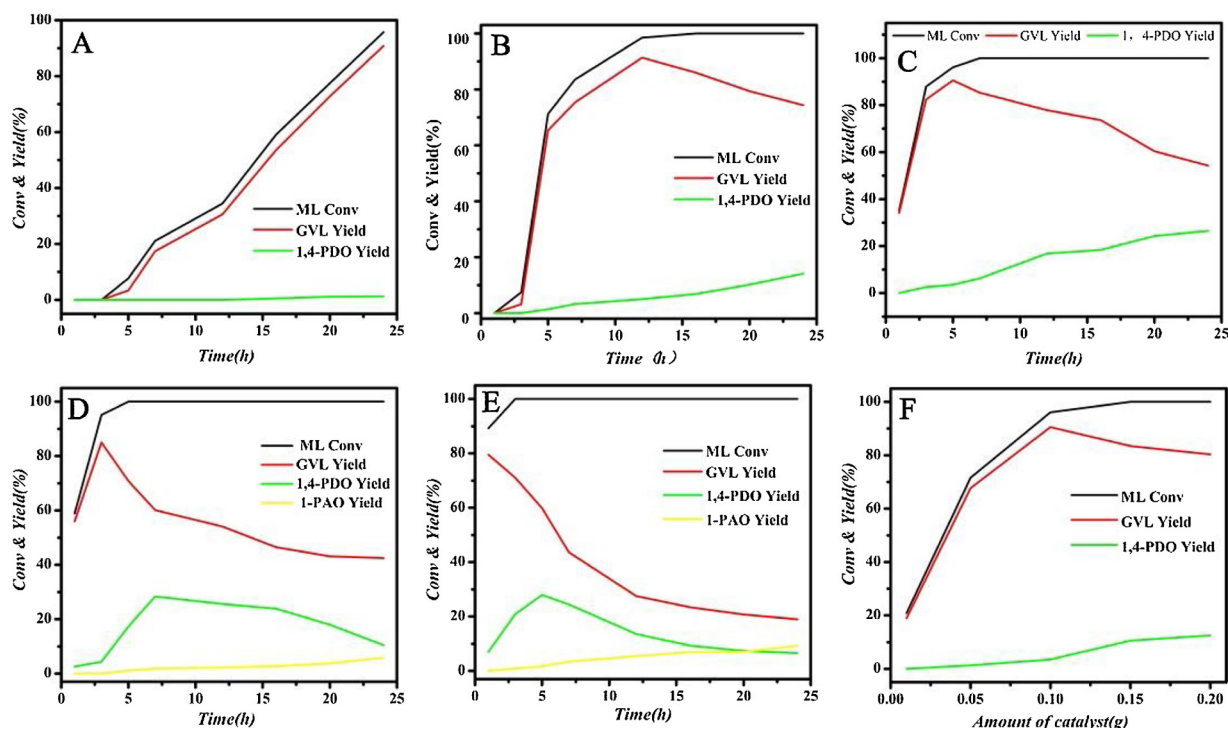


**Fig. 4.** Effect of different reaction conditions on the CTH reaction of ML. Effect of different reaction times on the CTH reaction of ML at 140 °C (A), 160 °C (B), 180 °C (C), 200 °C (D) and 220 °C (E). Reaction condition: catalyst (0.1 g), substrate (0.67 mmol), 2-PrOH (20 ml). Effect of different amount of  $\text{Cu}_2(\text{OH})_2\text{CO}_3/\text{AlOOH}$  on the CTH reaction of ML (F). Reaction condition: substrate (0.67 mmol), 2-PrOH (20 ml), 180 °C, 5 h.

the yield of 1,4-PDO increased with increasing amounts of the catalyst. At 0.15 g, the conversion of ML reached 100%, and at 0.20 g, the 1, 4-PDO yield reached a high value (12.72%), whereas the yield of  $\gamma$ -GVL began to decline after an optimal yield (90.51%) of 0.1 g was attributable to the further conversion of  $\gamma$ -GVL to 1, 4-PDO. Therefore, 0.1 g was chosen as the optimum amount of catalyst.

### 3.5. Scope of substrate and alcohols for production of $\gamma$ -GVL over $\text{Cu}_2(\text{OH})_2\text{CO}_3/\text{AlOOH}$

With the optimal reaction conditions obtained from above, the substrate and solvent scope of the CTH reaction are explored as revealed in Table 2. The CTH reaction with primary alcohols as the H-donors provided low yield of  $\gamma$ -GVL, which was similar to many previous works (Table 2, entry 1–5). [4,37] Primary alcohols were poor H-

**Table 2**  
Scope of substrate and alcohols for production of  $\gamma$ -GVL over  $\text{Cu}_2(\text{OH})_2\text{CO}_3/\text{AlOOH}$ .

Entry	Substrate	Alcohol	Conv (%)	GVL Yield (%)
1	ML	MeOH	15.77	0.39
2	ML	EtOH	14.81	0.12
3	ML	1-PrOH	18.99	1.57
4	ML	1-BuOH	32.27	2.20
5	ML	BnOH <sup>[a]</sup>	54.12	0.86
6	ML	t-BuOH <sup>[b]</sup>	39.42	0.47
7	ML	2-PrOH	96.07	90.51
8	ML	2-BuOH	97.81	89.37
9	ML	CyOH <sup>[c]</sup>	49.82	40.92
10	LA	2-PrOH	> 99	17.80
11	EL	2-PrOH	98.71	90.12
12	BL	2-PrOH	98.03	91.14

Conditions: catalyst(0.1 g), substrate(0.67 mmol), Alcohol (20 mL), 180 °C, 5 h. [a] BnOH stands for benzyl alcohol. [b] t-BuOH stands for T-butanol. [c] CyOH stands for Cyclohexanol.

donors in the CTH reaction owing to the difficult  $\beta$ -hydride removing after they shaped into alkoxy species on the surface of the catalyst. [45] Similarly, tertiary alcohols were also weak H-donors and failed to produce the corresponding carbonyl compounds because there were no hydrogens close to the hydroxyl group, which did not make the tertiary alcohols. As a result, hydrogen is not available for the CTH reaction, resulting in an inefficient CTH reaction with t-BuOH as the H-donors (Table 2, entry 6). It follows that the primary alcohols and tertiary alcohols are negative hydrogen donors for the CTH reaction. On the contrary, the secondary alcohols shew better performances, the CTH reaction with 2-BuOH gave a similar effect to that with 2-PrOH, obtained 89.37% and 90.51% yields of  $\gamma$ -GVL, respectively (Table 2, entries 7 and 8). Besides, CyOH was also a better H-donor for the CTH reaction, obtained 40.92% yield of  $\gamma$ -GVL. These results further confirm the aforementioned CTH reaction mechanism with secondary alcohols as hydrogen donors.<sup>9</sup>

We also studied the catalytic performance of the  $\text{Cu}_2(\text{OH})_2\text{CO}_3/\text{AlOOH}$  for various substrates. Ethyl levulinate (EL) and butyl levulinate (BL) were favourably converted to  $\gamma$ -GVL with 90.12% and 91.14% yield, respectively. However, the yield of  $\gamma$ -GVL achieved a very low yield (17.80%) when LA is subjected to the CTH reaction. This may be attributed to the fact that the acidity of LA causes LA to react with the AlOOH carrier, reducing the activity of the catalyst.

### 3.6. Reusability and heterogeneity of the catalyst

In addition to high catalytic activity, stability is also extremely important for heterogeneous catalysts. Therefore, reusability and heterogeneity were also investigated. In each cycle, the in situ reduced Cu/AlOOH catalyst was recovered by filtration, washed with fresh 2-PrOH (3 times), and then reused in next run. The results showed there was no obvious decrease in conversion and yield after five cycles, indicating that the catalyst is very stable (Fig. 5A). Leaching test of the catalyst was also explored (Fig. 5B). The reaction was stopped after 2 h, the catalyst was filtered out, and the reaction was then continued under the

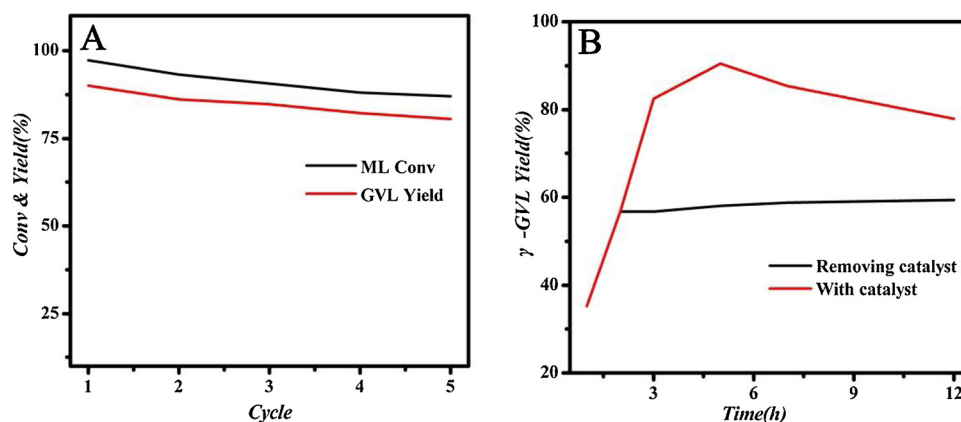


Fig. 5. Reusability (A) and leaching test (B) of the catalyst for the CTH reaction of ML. Reaction condition: catalyst (0.0631 g), substrate (0.67 mmol), 2-PrOH (20 mL), 180 °C, 5 h.

same conditions to examine whether the yield of  $\gamma$ -GVL continued to increase without the Cu/AlOOH catalyst. Clearly, the yield of  $\gamma$ -GVL after the removal of the catalyst no longer increased, indicating that the catalyst is heterogeneous. Meanwhile, trace of copper ions (0.11 ppm) in the solution after the reaction also indicated that the catalyst was heterogeneous and stable.

The stability of the catalyst is further analyzed by SEM, TEM and XPS. By comparing with SEM image of the spent catalyst after one cycle (Fig. 2C), the particle size of the catalyst became a bit larger after five times (Fig. 6A), which can be more clearly observed in the TEM image. The particle size of the spent catalyst was approximately 35 nm and 50 nm after one cycle and five cycles, respectively (Fig. 6B and C). In addition, the crystallinity of Cu became stronger after five cycles (Figure S7). Why these phenomena do not cause a significant drop in

the yield of  $\gamma$ -GVL? The answer is got from XPS analysis (Fig. 6D). After five cycles, for Cu 2p<sub>3/2</sub>, that the ratio of the peak areas of Cu<sup>0</sup>/Cu<sup>+</sup> species to Cu<sup>2+</sup> species significantly increased and that the satellite peaks disappeared indicated that there is more Cu<sup>0</sup> active sites in the spent catalyst. The emergence of more and more of Cu<sup>0</sup> active sites guarantees the stability of catalytic performance.

### 3.7. CTH reaction of carbonyl compounds over the Cu<sub>2</sub>(OH)<sub>2</sub>CO<sub>3</sub>/AlOOH

Inspired by the excellent catalytic performance of the prepared catalysts for the conversion of ML, we sought the possible results of the CTH reaction of other carbonyl compounds using the in situ reduced Cu/AlOOH catalyst from Cu<sub>2</sub>(OH)<sub>2</sub>CO<sub>3</sub>/AlOOH (Table 3). The results exhibited good catalytic activity on the examined compounds. In

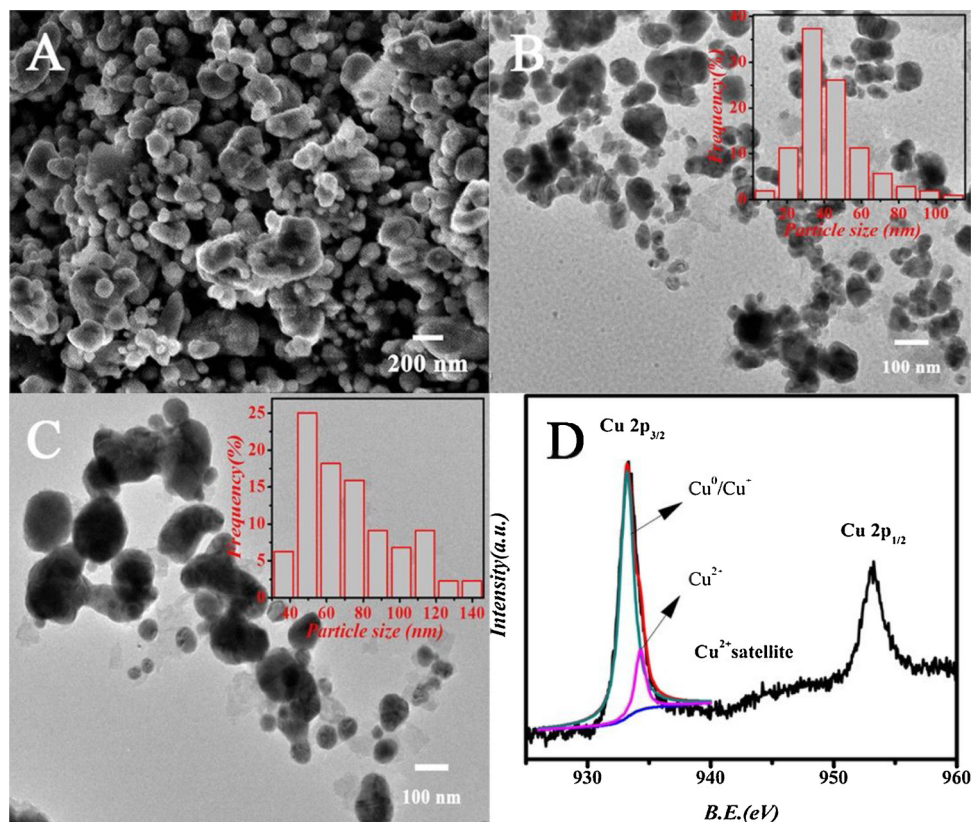
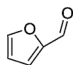
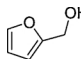
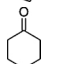
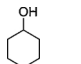
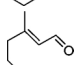
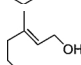
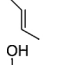
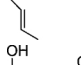
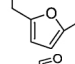
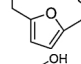
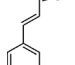
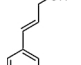


Fig. 6. SEM image of the in situ reduced Cu/AlOOH after five cycles (A), TEM image of the in situ reduced Cu/AlOOH after one cycle (B), TEM image of the in situ reduced Cu/AlOOH after five cycles (C), XPS analysis of the in situ reduced Cu/AlOOH after five cycles (D).

**Table 3**  
CTH reaction of carbonyl compounds over the  $\text{Cu}_2(\text{OH})_2\text{CO}_3/\text{AlOOH}$ .

Entry	Reactant	Main product	Temperature (°C)	Time (h)	Conv (%)	GVL Yield(%)
1 <sup>[a]</sup>			180	3	> 99	95.07
2 <sup>[b]</sup>			180	10	> 99	98.66
3 <sup>[c]</sup>			180	7	> 99	98.86
4 <sup>[d]</sup>			160	9	> 99	89.09
5 <sup>[e]</sup>			160	12	> 99	90.21
6 <sup>[f]</sup>			160	5	> 99	82.17

Conditions: catalyst(0.1 g), substrate(0.67 mmol), Alcohol (20 mL).

[a] Reactants and products are furfural and furfuryl alcohol respectively. [b] Reactants and products are cyclohexanone and cyclohexanol respectively. [c] Reactants and products are citral and citrate respectively. [d] Reactants and products are 5-hydroxymethylfurfural and 2,5-bis(hydroxymethyl)furan, respectively. [e] Reactants and products are cinnamaldehyde and cinnamyl alcohol respectively. [f] Reactants and products are acetophenone and  $\alpha$ -phenylethyl alcohol respectively.

particular, furfural, cyclohexanone and citral gave a great conversion (more than 99%) and satisfactory yields (95.07%, 98.66% and 98.86%, respectively) (Table 3, entry 1–3). For 5-hydroxymethylfurfural (HMF), cinnamaldehyde and acetophenone, the catalyst showed slightly lower activity (89.09%, 90.21% and 82.17%, respectively) (Table 3, entry 4–6). The reason for choosing to react at 160 °C was that the product would be further decomposed at 180 °C. For example, at 180 °C or above, 2,5-bis(hydroxymethyl)furan (BHMF) generated by the CTH reaction of HMF would further react to produce levulinic esters and  $\gamma$ -GVL, and a very small portion of C=C bond in the cinnamaldehyde would be hydrogenated, resulting in a slightly decrease in the yield of cinnamyl alcohol. In addition, the phenylethanol obtained from acetophenone would also be further dehydrated to ethyl benzene. From this point of view, the in situ reduced  $\text{Cu}/\text{AlOOH}$  catalyst from  $\text{Cu}_2(\text{OH})_2\text{CO}_3/\text{AlOOH}$  is efficient for the conversion of different carbonyl compounds.

#### 4. Conclusions

In summary, a one-step strategy for catalyst preparation and catalytic transfer hydrogenation (CTH) is proposed. The nano- $\text{Cu}/\text{AlOOH}$  catalyst prepared by in situ reduction of  $\text{Cu}_2(\text{OH})_2\text{CO}_3/\text{AlOOH}$  in 2-PrOH played an efficient role in the hydrogenation of ML to  $\gamma$ -GVL. The optimal reaction condition for  $\gamma$ -GVL is 180 °C for 5 h using the in situ reduced  $\text{Cu}_2(\text{OH})_2\text{CO}_3/\text{AlOOH}$  catalyst with Cu/Al molar ratio 3/1 (96.07% conversion of ML and 90.51% yield of GVL). And with the increase of reaction temperature and time,  $\gamma$ -GVL is further transformed to 1,4-PDO and 1-PAO.

The smaller particle size, better dispersibility and more low-valent copper species lead to better catalytic performance and cycle stability of the in situ reduced catalysts than the catalyst reduced with hydrogen for the CTH reaction. And in the in situ reduced catalysts, in situ reduced  $\text{Cu}/\text{AlOOH}$  has better catalytic activity than in situ reduced  $\text{Cu}/\text{Al}_2\text{O}_3$  because it can be reduced more easily in a short time. In addition, the catalyst also has good catalytic activity on the CTH reaction of

different carbonyl compounds. Overall, due to its advantages of low cost, high efficiency, good stability and simple preparation, etc., the  $\text{Cu}_2(\text{OH})_2\text{CO}_3/\text{AlOOH}$  catalyst holds a promising potential in catalyzing the CTH reaction of biomass.

#### Acknowledgements

This work was supported by grants from the National Natural Science Foundation of China (No. 21771086), Science and Technology Research Program of the Education Department of Jilin Province (JJKH20170778KJ), and Natural Science Foundation of Jilin Province, China (20180101293JC).

#### Appendix A. Supplementary data

Supplementary data associated with this article can be found, in the online version, at <https://doi.org/10.1016/j.mcat.2019.01.033>.

#### References

- J.Q. Bond, D.M. Alonso, W. Dong, R.M. West, J.A. Dumesic, Integrated catalytic conversion of *g*-Valerolactone to liquid alkenes for transportation fuels, *Science* 327 (5969) (2010) 1110–1114.
- Y. Sha, Z. Xiao, H. Zhou, K. Yang, Y. Song, N. Li, R. He, K. Zhi, Q. Liu, Direct use of humic acid mixtures to construct efficient Zr-containing catalysts for Meerwein-Ponndorf-Verley reactions, *Green Chem.* 19 (2017) 4829–4837.
- B. Liu, Z. Zhang, Catalytic conversion of biomass into chemicals and fuels over magnetic catalysts, *ACS Catal.* 6 (2015) 326–338.
- F. Li, L.J. France, Z. Cai, Y. Li, S. Liu, H. Lou, X. Li, Catalytic transfer hydrogenation of butyl levulinate to  $\gamma$ -valerolactone over zirconium phosphates with adjustable Lewis and Brønsted acid sites, *Appl. Catal. B: Environ.* 214 (2017) 67–77.
- K. Yan, Y. Yang, J. Chai, Y. Lu, Catalytic reactions of gamma-valerolactone: a platform to fuels and value-added chemicals, *Appl. Catal. B: Environ.* 179 (2015) 292–304.
- F. Ye, D. Zhang, T. Xue, Y. Wang, Y. Guan, Enhanced hydrogenation of ethyl levulinate by Pd-AC doped with Nb2O5, *Green Chem.* 16 (2014) 3951.
- P. Zhang, C.-H. Liu, L. Chen, J.-M. Chen, Y. Guan, P. Wu, Factors influencing the activity of SiO<sub>2</sub> supported bimetal Pd-Ni catalyst for hydrogenation of  $\alpha$ -angelicalactone: oxidation state, particle size, and solvents, *J. Catal.* 351 (2017) 10–18.
- A.S. Piskun, J.E. de Haan, E. Wilbers, H.H. van de Bovenkamp, Z. Tang, H.J. Heeres, Hydrogenation of levulinic acid to  $\gamma$ -Valerolactone in water using millimeter sized supported Ru catalysts in a packed bed reactor, *ACS Sustain. Chem. Eng.* 4 (2016) 2939–2950.
- J. Tan, J. Cui, T. Deng, X. Cui, G. Ding, Y. Zhu, Y. Li, Water-promoted hydrogenation of levulinic acid to  $\gamma$ -Valerolactone on supported ruthenium catalyst, *ChemCatChem* 7 (2015) 508–512.
- P. Pongrácz, B. Bartal, L. Kollár, L.T. Mika, Rhodium-catalyzed hydroformylation in  $\gamma$ -valerolactone as a biomass-derived solvent, *J. Organomet. Chem.* 847 (2017) 140–145.
- Z. Tian, C. Liu, Q. Li, J. Hou, Y. Li, S. Ai, Nitrogen- and oxygen-functionalized carbon nanotubes supported Pt-based catalyst for the selective hydrogenation of cinnamaldehyde, *Appl. Catal. A Gen.* 506 (2015) 134–142.
- Z. Tian, Q. Li, J. Hou, L. Pei, Y. Li, S. Ai, Platinum nanocrystals supported on CoAl mixed metal oxide nanosheets derived from layered double hydroxides as catalysts for selective hydrogenation of cinnamaldehyde, *J. Catal.* 331 (2015) 193–202.
- K.T. Li, R.H. Yen, Aqueous-phase Hydrogenolysis of glycerol over Re promoted Ru catalysts encapsulated in porous silica nanoparticles, *Nanomaterials (Basel)* 8 (2018) 153.
- V.K. Velisoju, N. Gutta, J. Tardio, S.K. Bhargava, K. Vankudoth, A. Chatla, S. Medak, V. Akula, Hydrodeoxygenation activity of W modified Ni/H-ZSM-5 catalyst for single step conversion of levulinic acid to pentanoic acid: an insight on the reaction mechanism and structure activity relationship, *Appl. Catal. A Gen.* 550 (2018) 142–150.
- W. Li, G. Fan, L. Yang, F. Li, Highly efficient vapor-phase hydrogenation of biomass-derived levulinic acid over structured nanowall-like nickel-based catalyst, *ChemCatChem* 8 (2016) 2724–2733.
- J. Zhang, J. Chen, Y. Guo, L. Chen, Effective upgrade of levulinic acid into  $\gamma$ -Valerolactone over an inexpensive and magnetic catalyst derived from hydrotalcite precursor, *ACS Sustain. Chem. Eng.* 3 (2015) 1708–1714.
- Z. Tian, Q. Li, Y. Li, S. Ai, Synthesis of nitrogen-doped carbon coated TiO<sub>2</sub> microspheres and its application as metal support in cinnamaldehyde hydrogenation, *Catal. Commun.* 61 (2015) 97–101.
- L. Jiang, P. Zhou, C. Liao, Z. Zhang, S. Jin, Cobalt nanoparticles supported on nitrogen-doped carbon: an effective non-noble metal catalyst for the upgrade of biofuels, *ChemSusChem* 11 (2018) 959–964.
- B. Chen, H. Guo, Z. Wan, X. Xu, H. Zhang, D. Zhao, X. Chen, N. Zhang, Efficient catalytic hydrogenation of butyl levulinate to  $\gamma$ -Valerolactone over a stable and magnetic CuNiCoB amorphous alloy catalyst, *Energy Fuels* 32 (2018) 5527–5535.
- B.P. Pinto, A.L.L. Fortuna, C.P. Cardoso, C.J.A. Mota, Hydrogenation of levulinic



- acid (LA) to  $\gamma$ -Valerolactone (GVL) over Ni–Mo/C catalysts and water-soluble solvent systems, *Catal. Lett.* 147 (2017) 751–757.
- [21] M. Grilc, B. Likozar, Levulinic acid hydrodeoxygenation, decarboxylation and oligomerization over NiMo/Al<sub>2</sub>O<sub>3</sub> catalyst to bio-based value-added chemicals: modelling of mass transfer, thermodynamics and micro-kinetics, *Chem. Eng. J.* 330 (2017) 383–397.
- [22] S. Ishikawa, D.R. Jones, S. Iqbal, C. Reece, D.J. Morgan, D.J. Willock, P.J. Miedzkiak, J.K. Bartley, J.K. Edwards, T. Murayama, W. Ueda, G.J. Hutchings, Identification of the catalytically active component of Cu–Zr–O catalyst for the hydrogenation of levulinic acid to  $\gamma$ -valerolactone, *Green Chem.* 19 (2017) 225–236.
- [23] R. Zhang, Y. Ma, F. You, T. Peng, Z. He, K. Li, Exploring to direct the reaction pathway for hydrogenation of levulinic acid into  $\gamma$ -valerolactone for future Clean-Energy Vehicles over a magnetic Cu–Ni catalyst, *Int. J. Hydrogen Energy* 42 (2017) 25185–25194.
- [24] J. Song, L. Wu, B. Zhou, H. Zhou, H. Fan, Y. Yang, Q. Meng, B. Han, A new porous Zr-containing catalyst with a phenate group: an efficient catalyst for the catalytic transfer hydrogenation of ethyl levulinate to  $\gamma$ -valerolactone, *Green Chem.* 17 (2015) 1626–1632.
- [25] A.H. Valekar, K.-H. Cho, S.K. Chitale, D.-Y. Hong, G.-Y. Cha, U.H. Lee, D.W. Hwang, C. Serre, J.-S. Chang, Y.K. Hwang, Catalytic transfer hydrogenation of ethyl levulinate to  $\gamma$ -valerolactone over zirconium-based metal–organic frameworks, *Green Chem.* 18 (2016) 4542–4552.
- [26] M. Chia, J.A. Dumesic, Liquid-phase catalytic transfer hydrogenation and cyclization of levulinic acid and its esters to gamma-valerolactone over metal oxide catalysts, *Chem. Commun.* 47 (2011) 12233–12235.
- [27] B. Cai, X.-C. Zhou, Y.-C. Miao, J.-Y. Luo, H. Pan, Y.-B. Huang, Enhanced catalytic transfer hydrogenation of ethyl levulinate to  $\gamma$ -Valerolactone over a robust Cu–Ni bimetallic catalyst, *ACS Sustain. Chem. Eng.* 5 (2016) 1322–1331.
- [28] Y. Yang, X. Xu, W. Zou, H. Yue, G. Tian, S. Feng, Transfer hydrogenation of methyl levulinate into gamma-valerolactone, 1,4-pentanediol, and 1-pentanol over Cu–ZrO<sub>2</sub> catalyst under solvothermal conditions, *Catal. Commun.* 76 (2016) 50–53.
- [29] H. Li, J. He, A. Riisager, S. Saravanamurugan, B. Song, S. Yang, Acid–Base bifunctional zirconium N-Alkyltriphosphate nanohybrid for hydrogen transfer of biomass-derived carboxides, *ACS Catal.* 6 (2016) 7722–7727.
- [30] J. He, H. Li, Y.-M. Lu, Y.-X. Liu, Z.-B. Wu, D.-Y. Hu, S. Yang, Cascade catalytic transfer hydrogenation–cyclization of ethyl levulinate to  $\gamma$ -valerolactone with Al–Zr mixed oxides, *Appl. Catal. A Gen.* 510 (2016) 11–19.
- [31] X. Tang, H. Chen, L. Hu, W. Hao, Y. Sun, X. Zeng, L. Lin, S. Liu, Conversion of biomass to  $\gamma$ -valerolactone by catalytic transfer hydrogenation of ethyl levulinate over metal hydroxides, *Appl. Catal. B: Environ.* 147 (2014) 827–834.
- [32] H.Y. Luo, D.F. Consoli, W.R. Gunther, Y. Román-Leshkov, Investigation of the reaction kinetics of isolated Lewis acid sites in Beta zeolites for the Meerwein–Ponndorf–Verley reduction of methyl levulinate to  $\gamma$ -valerolactone, *J. Catal.* 320 (2014) 198–207.
- [33] A.M. Hengne, C.V. Rode, Cu–ZrO<sub>2</sub> nanocomposite catalyst for selective hydrogenation of levulinic acid and its ester to  $\gamma$ -valerolactone, *Green Chem.* 14 (2012) 1064.
- [34] Q. Xu, X. Li, T. Pan, C. Yu, J. Deng, Q. Guo, Y. Fu, Supported copper catalysts for highly efficient hydrogenation of biomass-derived levulinic acid and  $\gamma$ -valerolactone, *Green Chem.* 18 (2016) 1287–1294.
- [35] Z. Li, X. Tang, Y. Jiang, Y. Wang, M. Zuo, W. Chen, X. Zeng, Y. Sun, L. Lin, Atom-economical synthesis of gamma-valerolactone with self-supplied hydrogen from methanol, *Chem. Commun.* 51 (2015) 16320–16323.
- [36] X. Tang, Z. Li, X. Zeng, Y. Jiang, S. Liu, T. Lei, Y. Sun, L. Lin, In situ catalytic hydrogenation of biomass-derived methyl levulinate to gamma-valerolactone in methanol, *ChemSusChem* 8 (2015) 1601–1607.
- [37] F. Wang, Z. Zhang, Catalytic transfer hydrogenation of furfural into furfuryl alcohol over magnetic  $\gamma$ -Fe<sub>2</sub>O<sub>3</sub>@HAP catalyst, *ACS Sustain. Chem. Eng.* 5 (2016) 942–947.
- [38] L. Xu, L. Li, Y. Ao, F. Long, J. Guan, Engineering highly efficient photocatalysts for hydrogen production by simply regulating the solubility of insoluble compound cocatalysts, *Int. J. Hydrogen Energy* 39 (2014) 11486–11493.
- [39] V. Koleva, V. Vassileva, Infrared study of some synthetic phases of malachite (Cu<sub>2</sub>(OH)<sub>2</sub>(CO<sub>3</sub>)-hydrozincite (Zn<sub>5</sub>(OH)<sub>6</sub>(CO<sub>3</sub>)<sub>2</sub>) series, *Spectrochim. Acta Part A* 58 (2002) 2051–2059.
- [40] Y. Dong, L. Zhang, Constructed 3D hierarchical porous wool-ball-like NiO-loaded AIOOH electrode materials for the determination of toxic metal ions, *Electrochim. Acta* 271 (2018) 27–34.
- [41] C. Hai, L. Zhang, Y. Zhou, X. Ren, J. Liu, J. Zeng, H. Ren, Phase transformation and morphology evolution characteristics of hydrothermally prepared boehmite particles, *J. Inorg. Organomet. Polym. Mater.* 28 (2017) 643–650.
- [42] Z. Wenjin, T. Zhengbin, C. Lijian, A. Shiyun, Humic acid-induced synthesis of hierarchical basic copper carbonate/AIOOH microspheres and its enhanced catalytic activity for 4-nitrophenol reduction, *Indian J. Chem.* (2016) 153–159.
- [43] W. Gong, C. Chen, Y. Zhang, H. Zhou, H. Wang, H. Zhang, Y. Zhang, G. Wang, H. Zhao, Efficient synthesis of furfuryl alcohol from H<sub>2</sub>-Hydrogenation/Transfer hydrogenation of furfural using sulfonate group modified Cu catalyst, *ACS Sustain. Chem. Eng.* 5 (2017) 2172–2180.
- [44] Z. Gao, L. Yang, G. Fan, F. Li, Promotional role of surface defects on carbon-supported ruthenium-based catalysts in the transfer hydrogenation of furfural, *ChemCatChem* 8 (2016) 3769–3779.
- [45] Z. Yang, Y.B. Huang, Q.X. Guo, Y. Fu, RANEY(R) Ni catalyzed transfer hydrogenation of levulinic acid esters to gamma-valerolactone at room temperature, *Chem. Commun.* 49 (2013) 5328–5330.